

# Helicity-dependent cross sections for the photoproduction of $\pi^0$ pairs from nucleons

M. Dieterle,<sup>1</sup> L. Witthauer,<sup>1</sup> A. Fix,<sup>2</sup> S. Abt,<sup>1</sup> P. Achenbach,<sup>3</sup> P. Adlarson,<sup>3</sup> F. Afzal,<sup>4</sup> P. Aguar Bartolome,<sup>3</sup> Z. Ahmed,<sup>5</sup> J.R.M. Annand,<sup>6</sup> H.J. Arends,<sup>3</sup> M. Bashkanov,<sup>7</sup> R. Beck,<sup>4</sup> M. Biroth,<sup>3</sup> N. Borisov,<sup>8</sup> A. Braghieri,<sup>9</sup> W.J. Briscoe,<sup>10</sup> F. Cividini,<sup>3</sup> C. Collicott,<sup>11</sup> S. Costanza,<sup>9</sup> A. Denig,<sup>3</sup> A.S. Dolzhikov,<sup>8</sup> E.J. Downie,<sup>10</sup> P. Drexler,<sup>3,12</sup> S. Gardner,<sup>6</sup> D. Ghosal,<sup>1</sup> D.I. Glazier,<sup>6,7</sup> I. Gorodnov,<sup>8</sup> W. Gradl,<sup>3</sup> M. Günther,<sup>1</sup> D. Gurevich,<sup>13</sup> L. Heijkenkjöld,<sup>3</sup> D. Hornidge,<sup>14</sup> G.M. Huber,<sup>5</sup> A. Käser,<sup>1</sup> V.L. Kashevarov,<sup>3,8</sup> S. Kay,<sup>7</sup> I. Keshelashvili,<sup>1</sup> R. Kondratiev,<sup>13</sup> M. Korolija,<sup>15</sup> B. Krusche,<sup>1,\*</sup> A. Lazarev,<sup>8</sup> V. Lisin,<sup>13</sup> K. Livingston,<sup>6</sup> S. Lutterer,<sup>1</sup> I.J.D. MacGregor,<sup>6</sup> D.M. Manley,<sup>16</sup> P.P. Martel,<sup>3,17</sup> V. Metag,<sup>12</sup> W. Meyer,<sup>18</sup> D.G. Middleton,<sup>17</sup> R. Miskimen,<sup>19</sup> E. Mornacchi,<sup>3</sup> C. Mullen,<sup>6</sup> A. Mushkarenkov,<sup>9,19</sup> A. Neganov,<sup>8</sup> A. Neiser,<sup>3</sup> M. Oberle,<sup>1</sup> M. Ostrick,<sup>3</sup> P.B. Otte,<sup>3</sup> D. Paudyal,<sup>5</sup> P. Pedroni,<sup>9</sup> A. Polonski,<sup>13</sup> A. Powell,<sup>6</sup> S.N. Prakhov,<sup>20</sup> G. Reicherz,<sup>18</sup> G. Ron,<sup>21</sup> T. Rostomyan,<sup>1</sup> A. Sarty,<sup>11</sup> C. Sfienti,<sup>3</sup> V. Sokhoyan,<sup>3</sup> K. Spieker,<sup>4</sup> O. Steffen,<sup>3</sup> I.I. Strakovsky,<sup>10</sup> T. Strub,<sup>1</sup> I. Supek,<sup>15</sup> A. Thiel,<sup>4</sup> M. Thiel,<sup>3</sup> A. Thomas,<sup>3</sup> M. Unverzagt,<sup>3</sup> Yu.A. Usov,<sup>8</sup> S. Wagner,<sup>3</sup> N.K. Walford,<sup>1</sup> D.P. Watts,<sup>7</sup> D. Werthmüller,<sup>1,6</sup> J. Wettig,<sup>3</sup> M. Wolfes,<sup>3</sup> and L.A. Zana<sup>7</sup>

(A2 Collaboration)

<sup>1</sup>*Department of Physics, University of Basel, CH-4056 Basel, Switzerland*

<sup>2</sup>*Laboratory of Mathematical Physics, Tomsk Polytechnic University, Tomsk, Russia*

<sup>3</sup>*Institut für Kernphysik, University of Mainz, D-55099 Mainz, Germany*

<sup>4</sup>*Helmholtz-Institut für Strahlen- und Kernphysik, University Bonn, D-53115 Bonn, Germany*

<sup>5</sup>*University of Regina, Regina, SK S4S-0A2 Canada*

<sup>6</sup>*SUPA School of Physics and Astronomy, University of Glasgow, Glasgow, G12 8QQ, UK*

<sup>7</sup>*SUPA School of Physics, University of Edinburgh, Edinburgh EH9 3JZ, UK*

<sup>8</sup>*Joint Institute for Nuclear Research, 141980 Dubna, Russia*

<sup>9</sup>*INFN Sezione di Pavia, I-27100 Pavia, Pavia, Italy*

<sup>10</sup>*Center for Nuclear Studies, The George Washington University, Washington, DC 20052, USA*

<sup>11</sup>*Department of Astronomy and Physics, Saint Mary's University, E4L1E6 Halifax, Canada*

<sup>12</sup>*II. Physikalisches Institut, University of Giessen, D-35392 Giessen, Germany*

<sup>13</sup>*Institute for Nuclear Research, RU-125047 Moscow, Russia*

<sup>14</sup>*Mount Allison University, Sackville, New Brunswick E4L1E6, Canada*

<sup>15</sup>*Rudjer Boskovic Institute, HR-10000 Zagreb, Croatia*

<sup>16</sup>*Kent State University, Kent, Ohio 44242, USA*

<sup>17</sup>*Mount Allison University, Sackville, New Brunswick E4L3B5, Canada*

<sup>18</sup>*Institut für Experimentalphysik, Ruhr Universität, 44780 Bochum, Germany*

<sup>19</sup>*University of Massachusetts, Amherst, Massachusetts 01003, USA*

<sup>20</sup>*University of California Los Angeles, Los Angeles, California 90095-1547, USA*

<sup>21</sup>*Racah Institute of Physics, Hebrew University of Jerusalem, Jerusalem 91904, Israel*

(Dated: July 14, 2020)

The double-polarization observable  $E$  and helicity-dependent cross sections  $\sigma_{1/2}$ ,  $\sigma_{3/2}$  have been measured for the photoproduction of  $\pi^0$  pairs off quasi-free protons and neutrons at the Mainz MAMI accelerator with the Crystal Ball/TAPS setup. A circularly polarized photon beam was produced by bremsstrahlung from longitudinally polarized electrons and impinged on a longitudinally polarized deuterated butanol target. The reaction products were detected with an almost  $4\pi$  covering calorimeter. The results reveal for the first time the helicity- and isospin-dependent structure of the  $\gamma N \rightarrow N\pi^0\pi^0$  reaction. They are compared to predictions from reaction models in view of nucleon resonance contributions and also to a refit of one model that predicted results for the proton and for the neutron target. The comparison of the prediction and the refit demonstrate the large impact of the new data.

PACS numbers: 13.60.Le, 14.20.Gk, 14.40.Aq, 25.20.Lj

The properties of the fundamental interactions between particles are reflected in the excitation spectrum of composite objects formed by them. Atomic spectroscopy has revealed the properties of the electromagnetic interaction in great detail. Nuclear spectroscopy was used to

study the strong interaction in nuclei on a length scale where nucleons and mesons are the relevant degrees of freedom. In the same way, the excitation spectrum of nucleons (protons and neutrons) is a major testing ground for the properties of the strong interaction in the regime where quark and gluon degrees of freedom dominate.

\* Corresponding author: email bernd.krusche@unibas.ch

Photoproduction of mesons is a powerful and versatile tool for the investigation of the nucleon excitation

spectrum, which reflects the properties of the strong interaction in the non-perturbative regime. Reactions like  $\gamma N \rightarrow N\pi, N\eta, N\omega, N\rho, N\eta'$  etc. have been studied in detail; however, single-meson production reactions are biased against states that do not decay directly to the nucleon ground state. In the constituent quark model, higher-lying nucleon resonances may de-excite preferentially in two-step processes involving an intermediate excited state [1]. The restriction to single-meson production could thus exclude entire multiplets of quark-model states from observation. The equivalent in nuclear physics would be to investigate only decays of excited states to the nuclear ground state by which we would have missed phenomena like vibrationally or rotationally excited collective nuclear states and many more.

Cascade decays via intermediate states require the investigation of multiple-meson final states. The simplest cases are pseudoscalar (PS) meson pairs like  $\pi\pi$  or  $\pi\eta$ . The reaction formalism and the sets of observables are discussed in [2, 3] and a field theoretic description of the process is given in [4]. For single-meson production, a ‘complete’ experiment, which allows the unique determination of the magnitudes and phases of all relevant amplitudes, requires the measurement of eight carefully chosen observables including single and double polarization observables as a function of two kinematic parameters (typically center-of-momentum (cm) energy and cm-polar angle) [5]. Photoproduction of PS meson pairs requires the measurement of eight observables as a function of five kinematic parameters to determine just the magnitudes of the amplitudes, and 15 observables have to be measured to fix also their phases [2].

Such a complete experiment for meson pairs is unrealistic; however, limited data sets can give valuable insights. Three-body final states offer powerful analysis strategies that are not available for single-meson production. Invariant-mass distributions of the particle pairs carry information about the decay chains (e.g. the invariant mass of the intermediate state). Polarization observables for circularly polarized beams, which depend only on the angle between reaction (photon - recoil nucleon) and production (meson - meson) plane, are easy to measure and robust against instrumental artefacts [6, 7].

Final states with *neutral* PS meson pairs are interesting because non-resonant background terms are suppressed. Recently,  $\pi^0\pi^0$  and  $\pi^0\eta$  pairs have been studied in detail, however, with somewhat different results. Non-resonant background is indeed small for  $\pi\eta$ -pairs which seem to be dominated below  $W \approx 2$  GeV by the decay of just a few isospin  $I = 3/2$   $\Delta$  states. (see Refs. [8–13]). Sequential resonance decays leave different imprints in the cross sections for  $\pi^0\pi^0$  and  $\eta\pi^0$  pairs and are thus complementary. The reaction chain  $\Delta^* \rightarrow \Delta\pi^0 \rightarrow N\pi^0\pi^0$  is suppressed with respect to  $N^* \rightarrow \Delta\pi^0 \rightarrow N\pi^0\pi^0$  by isospin by a factor of five, but  $\pi^0\eta$  sequences starting with a  $\Delta$  resonance are not isospin suppressed.

Photoproduction of neutral-pion pairs is still less understood than the  $\eta\pi^0$  final state although it has been

intensively studied experimentally. Measurements of unpolarized cross sections and polarization observables for proton and quasi-free neutron targets from threshold throughout the second and third nucleon resonance region [1, 6, 14–31] have been reported. However, there are unresolved issues even in the low-energy regime. Early data up to the second resonance region ( $E_\gamma \approx 800$  MeV) [14, 15] for  $\gamma p \rightarrow p\pi^0\pi^0$  were interpreted differently in models. Murphy and Laget [32] found a dominant contribution from the  $N(1440)1/2^+ \rightarrow N\sigma \rightarrow N\pi^0\pi^0$  decay of the Roper resonance by emission of the  $\sigma$  meson. This decay was negligible in the model of Gomez-Tejedor and Oset [33], which instead favored the  $N(1520)3/2^- \rightarrow \Delta\pi^0 \rightarrow N\pi^0\pi^0$  decay. More precise invariant-mass distributions of the  $\pi^0\pi^0$  and  $\pi^0N$  pairs [17] and the helicity dependence of the cross section [22] demonstrated the importance of the sequential  $N(1520)3/2^-$  decay. However, the GRAAL collaboration argued in Refs. [19, 23] again for a large  $N(1440)1/2^+ \rightarrow \sigma N$  contribution.

More precise cross-section data from the CBELSA/TAPS experiment [24, 25], covering a larger energy range, were analyzed with the Bonn-Gatchina (BnGa) coupled channel model. A dominant contribution from the broad  $\Delta(1700)3/2^-$  state was suggested from threshold up to the third resonance bump. The contribution from the  $N(1520)3/2^-$  was significant, while the one from the Roper resonance was small but required new parameters for this state. Further results from CBELSA/TAPS, [30, 31] have been used to extract properties of several higher lying states. However, this analysis also suggested a modified picture for the low-energy regime with a stronger contribution of the  $N(1680)5/2^+$  state. Results from the Crystal Ball/TAPS experiment [27, 28] have been analyzed with the Mainz MAID isobar model [34] and also with a partial-wave expansion of the amplitudes. The latter found evidence for an unexpectedly large contribution of the  $3/2^+$  partial wave in the threshold range.

The only data available so far for the  $n\pi^0\pi^0$  final state are cross sections from the GRAAL [23] and Crystal Ball/TAPS [29] experiment and the polarization observable  $I^\circ$  [6] also from Crystal Ball/TAPS.

In this Letter we report results from a precise measurement of the double-polarization observable  $E$  and helicity-dependent cross sections  $\sigma_{1/2}$  and  $\sigma_{3/2}$  for  $\pi^0\pi^0$  pairs off protons and neutrons at the Mainz MAMI accelerator [35]. In the formalism for pseudoscalar meson pairs given in [2] this observable would be  $P_z^\circ$ . The definition is identical to the one for the observable  $E$  in single meson production which we use as abbreviation. For a circularly polarized photon beam and a longitudinally polarized target, two different relative spin orientations, parallel or antiparallel, corresponding to the cross sections  $\sigma_{3/2}$  ( $\uparrow\uparrow$ ) and  $\sigma_{1/2}$  ( $\uparrow\downarrow$ ) are possible which are termed helicity-3/2 and helicity-1/2. This two configurations correspond for the excitation of nucleon resonances to the electromagnetic couplings  $A_{3/2}$  and  $A_{1/2}$  listed in the Review of Particle Physics (PDG) [36]. They are

related to the asymmetry  $E$  by

$$E = \frac{\sigma_{1/2} - \sigma_{3/2}}{\sigma_{1/2} + \sigma_{3/2}} = \frac{\sigma_{1/2} - \sigma_{3/2}}{2\sigma_0}, \quad (1)$$

where  $\sigma_0$  is the unpolarized cross section.

The experimental setup and the analysis procedures were described in Refs. [12, 37–39] which used the same data set for other reaction channels ( $N\eta$ ,  $N\pi^0$ , and  $N\eta\pi^0$ ) (most details were given in Ref. [38] for  $\eta$  production, the most similar analysis was for  $\eta\pi^0$  pairs in Ref. [12].) A detailed description of the present analysis will be given in a longer journal paper. Longitudinally polarized electron beams ( $e^-$  energy 1558 MeV) with polarization degrees between 83 and 85% produced circularly polarized bremsstrahlung photons. The energy-dependent polarization  $P_\odot$  of the photon beam followed from the polarization transfer formula given in Ref. [40] (see also [12, 37–39]). The photons were energy tagged with the Glasgow magnetic spectrometer [41]. The solid deuterated-butanol target contained longitudinally polarized deuterons (polarization degrees 55 - 62%). The polarization of the bound nucleons was corrected for nuclear effects as in Refs. [12, 37–39]. The detector was composed of the electromagnetic calorimeters Crystal Ball (CB) [42] and TAPS [43] covering almost the full solid angle [12, 37–39]. The target was placed in the center of the CB.

The identification of the  $p\pi^0\pi^0$  and  $n\pi^0\pi^0$  final states was done as in Refs. [12, 29] using the information from the charged particle detectors, invariant mass analysis (for the identification of  $\pi^0$  pairs), coplanarity and missing mass analysis (to reject background from higher multiplicity final states). Effects from nuclear Fermi motion were removed with a kinematic reconstruction of the final state of the reaction as discussed in [44].

The asymmetry  $E$  (Eq. (1)) can be directly derived from the measured count rates  $N_{1/2}, N_{3/2}$  for the two spin configurations

$$E = \frac{1}{P_\odot P_T} \cdot \frac{N_{1/2} - N_{3/2}}{(N_{1/2} - N_B) + (N_{3/2} - N_B)}. \quad (2)$$

Many systematic effects cancel in this ratio. The two major sources for systematic uncertainty are the beam ( $\pm 2.7\%$ ) and target ( $\pm 10\%$ ) [38] polarization degrees. The rest of the systematic effects comes from the non-polarized background rate  $N_B$  from the unpolarized nucleons bound in the carbon and oxygen nuclei of the butanol molecules. This background drops out only in the numerator but contributes to the denominator. It was eliminated in two different ways. The count rate  $N_B$  was directly measured with a special carbon-foam target that had the same geometry and density of the heavy nuclei as the butanol target. Asymmetries determined this way are labeled analysis (1). For this analysis, count rates from the butanol and carbon target have to be relatively normalized according to incident photon flux, target surface density, and detection efficiency. Since the target

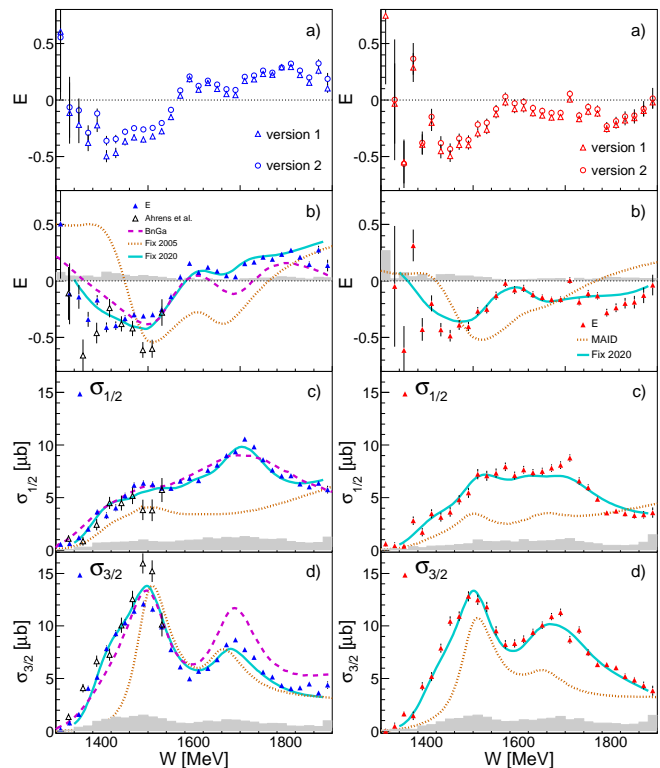


FIG. 1. Left-hand side: Reaction  $\gamma p \rightarrow p\pi^0\pi^0$ , quasi-free protons corrected for FSI. From top to bottom: (a) asymmetry  $E$  as function of invariant mass  $W$  integrated over all angles. Results from analysis (1) and (2). (b) average of  $E$  compared to previous low-energy data [22] and model results from BnGa [24] dashed (purple) curves and MAID [34] (brown) dotted curves and MAID refit (cyan) solid curves. (c)  $\sigma_{1/2}$  cross section compared to BnGa and MAID model, (d) same for  $\sigma_{3/2}$  cross section. Shaded (grey) histograms: systematic uncertainties. Right-hand side: Same for  $\gamma n \rightarrow n\pi^0\pi^0$ , no BnGa results available.

geometry was identical for both measurements and the target surface densities were adjusted almost identical (within ranges of a few per cent) they do not significantly contribute to systematic uncertainty and also the detection efficiency drops out. Only the effective photon flux for the two measurements matters which had an uncertainty of  $\approx 3\%$ . Alternatively, one can replace the denominator of Eq. (2) by the unpolarized cross section  $2\sigma_0$  measured with a liquid deuterium target (analysis (2)). For this analysis the different target densities of the liquid deuterium target and the solid butanol target have to be renormalized (typical uncertainties 4%). Also small effects (order of 1%) from detection efficiency might contribute because the length of the two targets was different. Finally, an effect could also arise from the tensor polarization of the butanol target which could lead to a difference between the total unpolarized cross section  $\sigma_0$  and the sum  $1/2(\sigma_{3/2} + \sigma_{1/2})$ . For consistency and minimization of systematic uncertainties both analyses used absolutely normalized cross sections determined from the

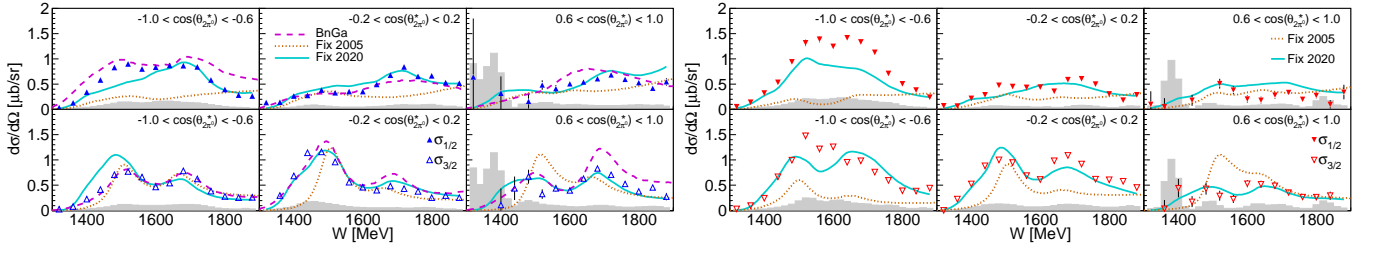


FIG. 2. Left-hand side: Differential cross sections for  $\gamma p \rightarrow p\pi^0\pi^0$  for different bins of the polar angle  $\Theta_{2\pi^0}^*$  as a function of the cm energy  $W$ . Upper row:  $\sigma_{1/2}$ , bottom row:  $\sigma_{3/2}$ . All results corrected for FSI (see text). Shaded (grey) histograms: systematic uncertainties. Notation for model curves as in Fig. 1. Right-hand side: Same for the reaction  $\gamma n \rightarrow n\pi^0\pi^0$ .

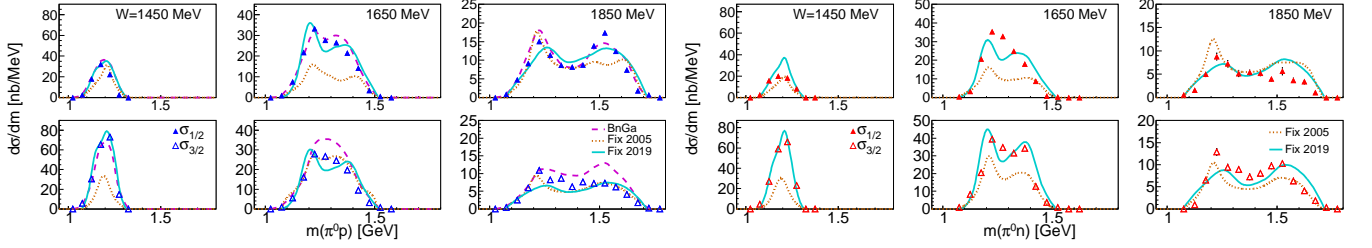


FIG. 3. Left-hand side: invariant-mass distributions of the  $p\pi^0$  pairs for different bins of  $W$  (1400 - 1500, 1600 - 1700, 1800 - 1900 MeV). Upper row  $\sigma_{1/2}$ , bottom row  $\sigma_{3/2}$ . Right-hand side: same for  $n\pi^0$ . Notation as in Fig. 1.

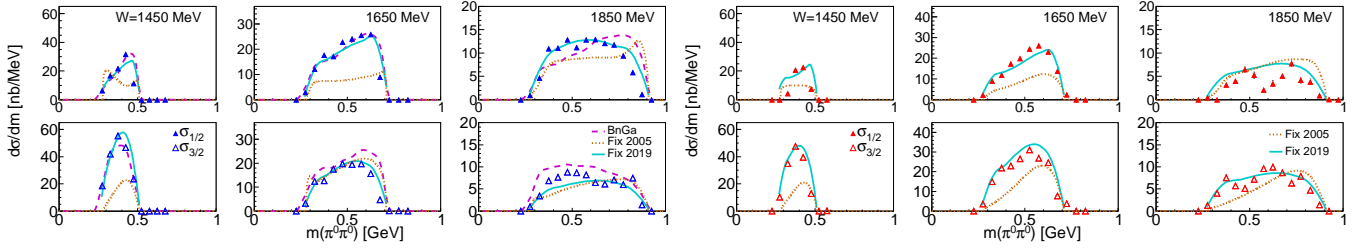


FIG. 4. Invariant-mass distributions of the  $\pi^0\pi^0$  pairs for different bins of  $W$  (1400 - 1500, 1600 - 1700, 1800 - 1900 MeV). Left-hand side for  $p\pi^0\pi^0$ , right-hand side for  $n\pi^0\pi^0$ . Upper rows  $\sigma_{1/2}$ , bottom row  $\sigma_{3/2}$ . Notation as in Fig. 1.

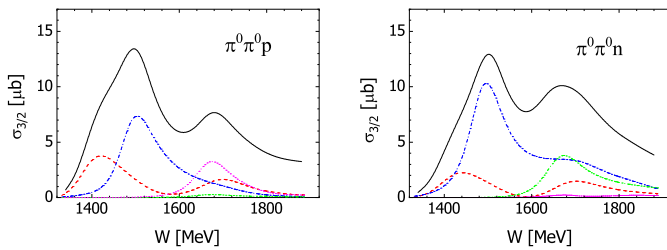


FIG. 5. (Color online) Contribution of several partial waves to the helicity-3/2 component of the total  $\pi^0\pi^0$  cross sections for protons (left hand side) and neutrons (right hand side), from the isobar model fit (see text). The contribution of the  $J^\pi = 3/2^-, 3/2^+, 5/2^-$  and  $5/2^+$  is shown by the dash-dotted (blue), dashed (red), double-dash-dotted (green), and the dotted (magenta) lines, respectively. The black solid line is the total helicity-3/2 cross section.

measured yields, photon fluxes, the target density, and the experimental detection efficiency constructed with

Monte Carlo simulations using the Geant4 package [45]. The best estimate of systematic uncertainty not related to polarization degrees comes from the comparison of this two analyses. The agreement between them is quite good, largest deviations are observed for the proton target below  $W=1.6$  GeV. Whether they arise from instrumental effects or target-tensor polarization cannot be decided. The same was previously observed for the  $N\pi^0$  [29],  $N\eta$  [37, 38], and  $N\pi\eta$  [12] final states.

So far, effects from final state interactions (FSI) on polarization observables have not been theoretically investigated. However, the results for other reaction channels for the  $E$  observable (single  $\pi^0$  production [39],  $\eta$  production [38]) did not show significant effects and also the measurement of a different polarization observable, the beam-helicity asymmetry  $I^\odot$  for  $\pi^0\pi^0$  and  $\pi^0\pi^+$  production off the proton showed no effects [6, 7], although absolute cross sections were effected in the 20% range. Also here (see below) the comparison to free proton data does not show significant effects (within the unfortu-

nately poorer statistical quality of the previous data). This is probably so, because FSI is not much sensitive to the initial polarization states and thus cancels in the asymmetry.

The helicity-dependent cross sections  $\sigma_{1/2}$  and  $\sigma_{3/2}$  were then derived from

$$\sigma_{1/2} = \sigma_0 \cdot (1 + E), \quad \sigma_{3/2} = \sigma_0 \cdot (1 - E). \quad (3)$$

The unpolarized cross sections  $\sigma_0$  were taken from [29]. For the  $p\pi^0\pi^0$  final state, the measurement with a liquid hydrogen target was used. For the  $n\pi^0\pi^0$  final state, the results measured with a liquid deuterium target were used after correction for FSI under the assumption that they are similar for reactions with bound protons and neutrons [29]. Under this assumption, the experimental data are compared to model results for free nucleons.

The most important results are summarized in Figs. 1-4. In the upper row (a) of Fig. 1, the results for  $E$  from analyses (1), (2) are compared. Systematic deviations are small which demonstrates that the treatment of the unpolarized background is well under control. For the following three rows (b)-(d) the two analyses have been averaged. Statistical uncertainties are highly correlated between the two analyses because these are dominated by the numerator of the asymmetry, which is identical for both analyses. Therefore the mean of the statistical uncertainties of the two analyses was used for the final results. At invariant masses below 1.5 GeV the results for  $E$  and  $\sigma_{1/2}$ ,  $\sigma_{3/2}$  for the quasifree proton are compared to free-proton results from Ref. [22]. They agree within statistical fluctuations, so that no indications of residual FSI effects were found.

Differential spectra are shown in Figs. 2,3,4 for angular distributions and the invariant meson-nucleon and meson-meson distributions. Only a few examples are shown, the full data set will be published in an upcoming paper. The angle  $\theta_{2\pi^0}^*$  is the polar angle of the combined two-pion system in the overall cm frame (i.e., within experimental resolution back-to-back with the recoil nucleon). The invariant-mass distributions of the pion-nucleon system are mostly sensitive to contributing intermediate resonances and the pion-pion invariant masses carry the signal from contributions such as  $N^* \rightarrow N\sigma$  involving the  $f_0(500)$  meson [36].

The experimental data are compared to the results from the BnGa model [24] and the MAID model [34]. The first is for double-pion production still restricted to the proton target. However, it fits also other reaction channels for the proton and also some (e.g. single  $\pi^0$  production) for the neutron [39, 46, 47]. The MAID model tries to describe all isospin channels for double-pion production in the framework of an isobar model with additional non-resonant backgrounds (e.g. Born terms) [34]. This model was refit to all available data for  $\gamma N \rightarrow \pi\pi N$  including the new helicity decomposition for  $\gamma N \rightarrow \pi^0\pi^0 N$ .

The comparison of this refit and the previous model results (see Figs. 1-4) demonstrate the large impact of the new data on the analysis. A full account of the im-

part of the new data on nucleon resonance parameters will be given in a journal paper. Here, we discuss as example only the helicity-3/2 contributions of the lowest partial waves. The new fit results in the partial waves  $3/2^-$ ,  $3/2^+$ ,  $5/2^-$ , and  $5/2^+$  are shown in Fig. 5. Previous fits to the proton data [24, 34] suggested that substantial strength of the second nucleon resonance bump around  $W=1500$  MeV comes from a sequential decay of the  $N(1520)3/2^-$  resonance via the  $\Delta(1232)$  state ( $3/2^-$  wave). This is confirmed and an even more dominant contribution of this partial wave is found for the neutron target. The  $3/2^+$  wave has contributions from the  $N(1720)3/2^+$  state. However, it is also important in the threshold region where no resonance with this quantum numbers exists. The importance of this wave at low energies was already noted in Ref. [28], but it is quantitatively improved by the present data. The two-humped structure in Fig. 5 is mainly the result of interference of the  $N(1720)3/2^+$  resonance with a wide non-resonant background. There is, however, no clear understanding of the nature of the strong background contribution. As discussed in Ref. [28] at least part of it is related to the  $\pi^+\pi^- \rightarrow \pi^0\pi^0$  rescattering effect.

The most interesting part is the third resonance region around  $W=1700$  MeV. So far, there is no agreement between different models about its origin. The double-hump structure of the cross section for the proton is explained in Refs. [24, 25] by an interference between the two  $3/2^-$  waves with isospin  $I=1/2, 3/2$ , where the  $I=3/2$  part dominates. On the contrary, in Ref. [34] the peak around  $W=1700$  MeV is for the proton mainly assigned to the  $N(1680)5/2^+$  state and significant contributions from the  $3/2^-$ ,  $I=3/2$  state were excluded. The dominance of  $N(1680)5/2^+$  was also found in a more recent analysis of the  $\gamma p \rightarrow \pi^0\pi^0 p$  data in Ref. [31] and the present results (see left-hand side of Fig. 5) for the proton are also in agreement with it. However, although the excitation functions of the unpolarized cross section for the proton and neutron target look quite similar, the present data reveal that the origin of the second maximum is much different. For the neutron, the fit to angular and invariant mass distributions in the second peak reveals a dominant contribution of the  $5/2^-$  wave which can be attributed to the  $N(1675)5/2^-$  state (see right-hand side of Fig. 5) and rejects almost completely contributions from the  $N(1680)5/2^+$ .

## ACKNOWLEDGMENTS

We wish to acknowledge the outstanding support of the accelerator group and operators of MAMI. This work was supported by Schweizerischer Nationalfonds (200020-156983, 132799, 121781, 117601), Deutsche Forschungsgemeinschaft (SFB 443, SFB 1044, SFB/TR16), the INFN-Italy, the European Community-Research Infrastructure Activity under FP7 programme (Hadron Physics, grant agreement

No. 227431), the UK Science and Technology Facilities Council (ST/J000175/1, ST/G008604/1, ST/G008582/1, ST/J00006X/1, and ST/L00478X/1), the Natural Sciences and Engineering Research Council (NSERC, FRN: SAPPJ-2015-00023), Canada. This material is based upon work also supported by the U.S.

Department of Energy, Office of Science, Office of Nuclear Physics Research Division, under Award Numbers DE-FG02-99-ER41110, DE-FG02-88ER40415, DE-FG02-01-ER41194, and de-sc0014323 and by the National Science Foundation, under Grant Nos. PHY-1039130 and IIA-1358175.

- 
- [1] A. Thiel *et al.*, Phys. Rev. Lett. **114**, 091803 (2015).  
 [2] W. Roberts and T. Oed, Phys. Rev. C **71**, 055201 (2005).  
 [3] A. Fix and H. Arenhovel, Phys. Rev. C **83**, 015503 (2011).  
 [4] H. Haberzettl, K. Nakayama, and Y. Oh Phys. Rev. D **99**, 053001 (2019).  
 [5] W.T. Chiang, F. Tabakin, Phys. Rev. C **55**, 2054 (1997).  
 [6] M. Oberle *et al.*, Phys. Lett. B **721**, 237 (2013).  
 [7] M. Oberle *et al.*, Eur. Phys. J. A **50**, 54 (2014).  
 [8] E. Gutz *et al.*, Eur. Phys. J. A **50**, 74 (2014).  
 [9] B. Krusche and C. Wilkin, Prog. Part. Nucl. Phys. **80**, 43 (2015).  
 [10] A. Käser *et al.*, Phys. Lett. B **748**, 244 (2015).  
 [11] A. Käser *et al.*, Eur. Phys. J. A **52**, 272 (2016).  
 [12] A. Käser *et al.*, Phys. Lett. B **786**, 305 (2018).  
 [13] V. Sokhoyan *et al.*, Phys. Rev. C **97**, 055212 (2018).  
 [14] A. Braghieri *et al.*, Phys. Lett. B **363**, 46 (1995).  
 [15] F. Härter *et al.*, Phys. Lett. B **401**, 229 (1997).  
 [16] B. Krusche *et al.*, Eur. Phys. J. A **6**, 309 (1999).  
 [17] M. Wolf *et al.*, Eur. Phys. J. A **9**, 5 (2000).  
 [18] V. Kleber *et al.*, Eur. Phys. J. A **9**, 1 (2000).  
 [19] Y. Assafiri *et al.*, Phys. Rev. Lett. **90**, 222001 (2003).  
 [20] B. Krusche and S. Schadmand, Prog. Part. Nucl. Phys. **51**, 399 (2003).  
 [21] M. Kotulla *et al.*, Phys. Lett. B **578**, 63 (2004).  
 [22] J. Ahrens *et al.*, Phys. Lett. B **624**, 173 (2005).  
 [23] J. Ajaka *et al.*, Phys. Lett. B **651**, 108 (2007).  
 [24] A. V. Sarantsev *et al.*, Phys. Lett. B **659**, 94 (2008).  
 [25] U. Thoma *et al.*, Phys. Lett. B **659**, 87 (2008).  
 [26] D. Krambrich *et al.*, Phys. Rev. Lett. **103**, 052002 (2009).  
 [27] F. Zehr *et al.*, Eur. Phys. J. A **48**, 98 (2012).  
 [28] V. L. Kashevarov *et al.*, Phys. Rev. C **85**, 064610 (2012).  
 [29] M. Dieterle *et al.*, Eur. Phys. J. A **51**, 142 (2015).  
 [30] V. Sokhoyan *et al.*, Phys. Lett. B **746**, 127 (2015).  
 [31] V. Sokhoyan *et al.*, Eur. Phys. J. A **51**, 95 (2015).  
 [32] L. Y. Murphy and J. M. Laget, DAPHNIA/SPhN, 96-10 (1996).  
 [33] J. A. Gomez Tejedor and E. Oset, Nucl. Phys. A **600**, 413 (1996).  
 [34] A. Fix and H. Arenhövel, Eur. Phys. J. A **25**, 115 (2005).  
 [35] K.-H. Kaiser *et al.*, Nucl. Instr. Meth. A **593**, 159 (2008).  
 [36] M. Tanabashi *et al.*, Phys. Rev. D **98**, 030001 (2018).  
 [37] L. Witthauer *et al.*, Phys. Rev. Lett. **117**, 132502 (2016).  
 [38] L. Witthauer *et al.*, Phys. Rev. C **95**, 055201 (2017).  
 [39] M. Dieterle *et al.*, Phys. Lett. B **770**, 523 (2017).  
 [40] H. Olsen and L. C. Maximon, Physical Review **114**, 887 (1959).  
 [41] J.C. McGeorge *et al.*, Eur. Phys. J. A **37**, 129 (2008).  
 [42] A. Starostin *et al.*, Phys. Rev. C **64**, 055205 (2001).  
 [43] A.R. Gabler *et al.*, Nucl. Inst. and Meth. A **346**, 168 (1994).  
 [44] B. Krusche, Eur. Phys. J. Special Topics **198**, 199 (2011).  
 [45] S. Agostinelli *et al.*, Nucl. Instr. Meth. A **506**, 250 (2003).  
 [46] M. Dieterle *et al.*, Phys. Rev. Lett. **112**, 142001 (2014).  
 [47] M. Dieterle *et al.*, Phys. Rev. C **97**, 065205 (2018).